The Somali Current response to the Southwest Monsoon: the relative importance of local and remote forcing

by David L. T. Anderson[1] and Philip B. Rowlands[1]

ABSTRACT

A simple model of the Somali current is formulated which allows both local longshore forcing and remote east-west forcing. Asymptotic solutions for the pressure perturbation and velocity fields are obtained for both cases and the sensitivity of the boundary response to changes in the shape and position of the forcing is examined. The local forcing drives a flow whose north-south velocity increases linearly with time and the remote forcing, a flow in which the north-south velocity increases quadratically. These results will break down when dissipative effects or strong nonlinearities develop. For the case of local forcing which is particularly strong between 10°N-12°N a nonlinear calculation is performed. This allows upwelling to develop locally in the vicinity of the strong forcing region in accord with observation, an effect which cannot be explained by a linear model since in such a model coastal Kelvin waves smear out the local response. The conclusions are that initially the local forcing is much more important than remote forcing but that, for the nondissipative case, remote forcing will ultimately become important. The separation point of the Somali current we suggest is a delicate balance between remote forcing trying to produce a southward current in this area and local nonlinear dynamics trying to establish a poleward flow. The model is compared with observations and appears to agree reasonably well. Baroclinic and shear instability and dissipative effects, all of which could be important in the boundary region, have been ignored. The fact that the Somali coast does not lie north-south has only partly been accounted for. However, the local winds used are those blowing along the shore and thus the main dynamic effects of the nonmeridional direction of this boundary have probably been included.

1. Introduction

This paper develops a linear, inviscid theory for the generation of western boundary currents at the equator; the techniques described in Anderson and Rowlands (1976) are modified for this purpose. The forcing mechanism is supposed to be the onset of a strong, steady wind the important components of which are the longshore stress near the coast and the zonal stress near the equator.

It is shown that the local longshore wind stress leads to a longshore current which increases linearly with time and that this is initially the dominant response.

1. Department of Applied Mathematics and Theoretical Physics, University of Cambridge, Silver Street, Cambridge, England, CB3 9EW.

The remote wind stress gives rise to a longshore current which increases quadratically with time, and which thus becomes the dominant feature later. The former mechanism for the generation of the Somali Current by the onset of the Southwest Monsoon was considered by Cox (1970) and the latter by Lighthill (1969). These authors concluded that the response to local winds is immediate (Cox) while the response to remote winds is less rapid (~ 1 month: Lighthill), a conclusion supported by the observations of Leetmaa (1972, 1973). The present work clarifies this situation and gives more detailed predictions of the likely response.

The theory is applied to the Somali Current in the latter part of this paper. Several possible forms of the wind stress are considered (there are few good measurements), and the sensitivity of results to different stress patterns analyzed. This leads to the conclusion that the response to the local forcing is rather insensitive to its exact distribution, while the response to the remote stress is more sensitive. These predictions are then compared with various observations and it is concluded that the main features of the development of the Somali Current are described well by the present theory, except in the region just south of Cape Guardafui where a strong upwelling region is observed but is not predicted by our theory. A simple nonlinear theory is then applied to this region, which corresponds to a strong low-level jet blowing off the African continent and parallel to the shore (Findlater, 1974). This indicates that an increase in upwelling is to be expected in this area. The details of this model are given in the Appendix.

2. General Formulation

The model used consists of a semi-infinite ocean basin with a flat bottom and a vertical western coast which is oriented exactly north-south. Following Anderson and Rowlands (1976), the equations we will use are

$$2r^{m-1}{}_{ttt} - 2r^{m-1}{}_{xxt} + (2m+1)r^{m-1}{}_{t} - r^{m-1}{}_{x} = -2\,X^{m-1}{}_{tt} - 2X^{m-1}{}_{xt} + m(m+1)X^{m+1} - (m+1)X^{m-1} - 2m\,Y^{m}{}_{t} - 2m\,Y^{m}{}_{x} \tag{2.1}$$

$$2r^{m-1}{}_{tt} - 2r^{m-1}{}_{xt} - m(m+1)\,q^{m+1} + mr^{m-1} = -2X^{m-1}{}_{t} - 2mY^{m} \tag{2.2}$$

$$2v^{m}{}_{t} + (m+1)\,q^{m+1} - r^{m-1} = 2Y^{m} \tag{2.3}$$

where the eastward, southward velocities (u,v), perturbation pressure p, and body force (X,Y) equivalent to wind-stress forcing (Lighthill, 1969) have been separated into vertical modes, and then expanded as series of parabolic cylinder functions, e.g.

$$r = \sum_{m=0}^{\infty} r^{m} D_{m}(y)$$

where $r = p - u$, $q = p + u$

Length has been scaled by the equatorial radius of deformation, $a_n = (c_n/2\beta)^{\frac{1}{2}}$, time by a_n/c_n and velocity by c_n (the speed of propagation of gravity waves in the

*n*th vertical mode in the absence of rotation). The equations hold for each vertical mode, but we will consider primarily the first baroclinic mode which is the main contribution to upwelling (it corresponds to vertical displacement of the thermocline as a whole; other modes will tend to distort the vertical structure of the thermocline) and which is also the mode most easily forced by a surface wind stress (Lighthill, 1969). It should be noted that for this mode u,v have the same sign as the surface current, and positive p corresponds to downward displacement of the thermocline. For this first baroclinic mode $c_n \sim 2m\ s^{-1}$, $a_n \sim 200$ km and thus 1 unit of dimensionless time corresponds closely to 1 day and 1 unit of dimensionless distance to 2° of latitude or longitude.

At the western boundary $u = 0$ implying $q^m = r^m$. The flow of energy is toward the equator at a western boundary via trapped Kelvin waves. Moore (1968) has shown that (2.2) can then be used as a boundary condition to determine r^{m-1} knowing $r^{m+1} = (q^{m+1})$. Eq. (2.3) will be used as an equation for determining v^m, once one has solved (2.1) for r^{m-1}.

It is convenient to consider separately the two types of forcing X,Y and to examine first the long time asymptotic behavior of the solutions. The details of how this asymptotic solution is obtained are discussed in section 3. The method of solution is similar to that given in Anderson and Rowlands (1976). The Laplace transform with respect to time of (2.1)-(2.3) is first taken and then the solution for $\hat{r}^{m-1}$ is obtained which is of the form (where the caret symbol denotes the Laplace transform of a variable, i.e. $\hat{r} = \int_0^\infty re^{-st}dt$).

$$\hat{r}^{m-1} = A^{m-1} \quad \exp(k_-{}^{m-1}x) + I^{m-1} \tag{2.4}$$

where

$$k_-{}^{m-1} = -\{1+[1+16(m+\tfrac{1}{2})s^2 + 16s^4]^{\frac{1}{2}}\}/4s \tag{2.5}$$

and

$$k_+{}^{m-1} = -\{1-[1+16(m+\tfrac{1}{2})s^2 + 16s^4]^{\frac{1}{2}}\}/4s\ .$$

Exact determination of A^{m-1} and I^{m-1}, a particular integral of (2.1), cannot be given until a particular form of X,Y forcing has been specified.

3. Solution for steady north-south forcing

We neglect the variation of Y with x, on the assumption that most longshore winds extend from the coast a distance greater than the baroclinic radius of deformation (~ 100 km at 2°N).

Then

$$I^{m-1} = \frac{-2m\hat{Y}^m}{(2s^2+2m+1)} \tag{3.1}$$

where we have assumed that the Y forcing is imposed at time $t = 0$ and is steady thereafter (i.e. $\hat{Y}^m = Y^m/s$). The solution for $\hat{r}^{m-1}$ is

$$\hat{r}^{m-1} = \frac{[m(m+1)\hat{r}^{m+1}|_{x=0} - 2m(m+1)(2m+2s^2+1)^{-1}\hat{Y}^m]\exp(k_-{}^{m-1}x)}{2s^2+m-2sk_-{}^{m-1}} - \frac{2m\hat{Y}^m}{2s^2+2m+1} . \tag{3.2}$$

The longterm behavior of (3.2), (2.2), (2.3) can be obtained by letting $s \to 0$. Then (3.2) becomes, at $x = 0$,

$$\hat{r}^{m-1}|_{x=0} = m\,\hat{r}^{m+1}|_{x=0} - 4m(2m+1)^{-1}\hat{Y}^m \tag{3.3}$$

and

$$\hat{p}|_{x=0} = \frac{1}{s}\sum_{m=0}^{\infty} G^m D_m(y) \tag{3.4}$$

where

$$G^m = (m+1)G^{m+2} - 4(m+1)(2m+3)^{-1}Y^{m+1} . \tag{3.5}$$

From (2.3) we have

$$\hat{v}|_{x=0} = \frac{1}{2s^2}\sum_{m=0}^{\infty}\{G^{m-1} - (m+1)G^{m+1} + 2Y^m\}D_m(y) \tag{3.6}$$

The asymptotic form of (3.4) and (3.6) indicates that, irrespective of the longshore dependence of local longshore forcing, the thermocline displacement will asymptote to a steady value at the coast while the longshore current will increase linearly with time. A more detailed time dependence will be considered later when we apply this theory to the Somali Current.

The asymptotic form of (3.2) away from the coast is given by

$$\hat{r}^m = \tilde{r}^m{}_B e^{-x/2s} - 2(m+1)(2m+3)^{-1}\hat{Y}^{m+1} \tag{3.7}$$

where the second term on the right-hand side is the solution in the absence of a coast, and the first term is the correction due to the presence of the coast. The x,t dependence of such boundary response terms is independent of m and thus these terms may be easily summed to give r. A similar result holds for q. Using the recurrence relations and differential equations for parabolic cylinder functions (Abramowitz and Stegun, 1965), it is possible to show that the sum of the last terms in (3.7) is the solution which tends to zero as $y \to \pm\infty$ of the differential equation

$$\hat{r}''_I - (1+\tfrac{1}{4}y^2)\hat{r}_I = \hat{Y}' + \tfrac{1}{2}y\hat{Y} . \tag{3.8}$$

Here a prime means differentiation with respect to y. Similarly the total solution at $x = 0$ is given by

$$\hat{r}'' + \tfrac{1}{2}\,y\hat{r}' - \tfrac{1}{2}\,\hat{r} = \hat{Y}' + \tfrac{1}{2}\,y\hat{Y} - \tfrac{1}{2}\,\hat{r}_I \tag{3.9}$$

and $\hat{r} \to 0$ as $y \to \pm\infty$. Thus $\tilde{r}_B$ may be found from (3.7) and the solution for r reconstructed everywhere.

A similar method applied to q gives

$$\hat{q}''_I + (1-\tfrac{1}{4}y^2)\hat{q}_I = \hat{Y}' - \tfrac{1}{2}y\hat{Y} \tag{3.10}$$

and

$$y\,\tilde{q}'_B - 2\tilde{q}''_B - (\tilde{q}_B - \tilde{q}^0{}_B\, D_0(y)) = y\hat{Y} - 2\hat{Y}' - y\,\hat{q}'_I + 2\hat{q}''_I \tag{3.11}$$

with $\hat{q}_I, \tilde{q}_B \to 0$ as $y \to \pm\,\infty$.

The term $\tilde{q}^0{}_B\, D_0(y)$ is just the equatorial Kelvin wave, which has a different x,t dependence from the other contributions to $\tilde{q}_B$.

Inversion of the Laplace transforms gives

$$r \sim r_B\, J_0[(2xt)^{\frac{1}{2}}] + r_I \tag{3.12}$$

and

$$q \sim (q_B - q^0{}_B\, D_0(y))\, J_0[(2xt)^{\frac{1}{2}}] + q^0{}_B D_0(y) + q_I \tag{3.13}$$

as $t \to \infty$, where J_0 is the zero-order Bessel function of the first kind. Thus u, p are given as functions of the single variable xt. This indicates the existence of a narrowing boundary layer. The longshore flow derived from this is

$$v/t \sim (2/xt)^{\frac{1}{2}}\, J_1[(2xt)^{\frac{1}{2}}] f_B(y) + f_I(y) \tag{3.14}$$

where f_B and f_I are functions of y which can be related to q_B, r_B via (2.3).

4. Solution for steady east-west forcing

Here we restrict the forcing to zero at the coast to a distance a from the coast. Thus between the coast and the forcing region we have westward propagating Rossby waves and a boundary response. Then in (2.4) we have

$$I^{m-1} = \frac{[(-2s^2-2k_+{}^{m-1}\,s-m-1)X^{m-1} + m(m+1)X^{m+1}]\exp[k_+{}^{m-1}(x-a)]}{2sk_+{}^{m-1}(k_+{}^{m-1}-k_-{}^{m-1})} \tag{4.1}$$

and

$$A^{m-1} = \frac{(2sk_+{}^{m-1}-2s^2-m)I^{m-1} + m(m+1)\,\hat{r}^{m+1}|_{x=0}}{(2s^2+ m-2sk^m{}_-)} \tag{4.2}$$

to the west of the forcing region.

The solution at $x = 0$ as $s \to 0$ is given by

$$\hat{p} = F(y)/s^2 \tag{4.3}$$

and

$$\hat{v} = \Phi(y)/2s^3 \tag{4.4}$$

where F, Φ are some functions of y related to the forcing by

$$F^{m-1} = (mX^{m+1}-X^{m-1})/(2m+1) + mF^{m+1}$$
$$\Phi^m = -\,(m+1)F^{m+1} + F^{m-1},\ \Phi^0 = -\,F^1$$

and Φ is the sum over all m of $\Phi^m D_m(y)$ etc. Eqs. (4.3), (4.4) show that for east-west forcing the thermocline displacement increases linearly with time, while the boundary current increases quadratically.

$$
\begin{aligned}
&q_I \sim \tilde{q}_I t \\
&r_I \sim \tilde{r}_I t \\
&q_B{}^0 D_0(y) \sim \tilde{q}_B{}^0 D_0(y) t \\
&r_B \sim \tilde{r}_B (2t/x)^{\frac{1}{2}} J_1[(2xt)^{\frac{1}{2}}] \\
&q_B - q^0{}_B D_0(y) \sim (\tilde{q}_B - \tilde{q}^0{}_B D_0(y))(2t/x)^{\frac{1}{2}} J_1[(2xt)^{\frac{1}{2}}]
\end{aligned}
\tag{4.10}
$$

Again the boundary response terms give a narrowing boundary layer.

5. A model of the Somali Current

We now apply this theory to the western part of the Indian ocean, and in particular to the generation of the Somali Current by the onset of the Southwest Monsoon.

Leetmaa (1972, 1973) has examined the response of this current (which flows northward only during the Southwest Monsoon) in 1970 and 1971. He found that the surface flow is northward before the Southwest Monsoon is in evidence in mid-ocean. Thus the mechanism proposed by Lighthill (1969) (generation by winds in mid-ocean) cannot be responsible for the initial development of the current. This agrees with the theory presented above, which indicates that local winds drive the current initially, while later in the season effects due to the remote component of the Monsoon are likely to dominate.

For the initial response we consider a north-south wind stress near the coast, and as noted in §3 we neglect any zonal variation of this wind. Fieux (1975) indicates a very rapid onset of this wind (~ 1-5 days) while Leetmaa (1972, 1973) suggests that it takes a few days longer. With times of this order it is questionable whether a step function onset of the wind is sufficiently accurate, as it takes only about 6 days for a coastal Kelvin wave to reach the equator from the Gulf of Aden. However, we are interested here only in the long-time asymptotic behavior of the ocean, and for this purpose it is unimportant exactly how we impose the wind; what is important is that the wind used in the model should have the same long-term behavior as the real wind (effectively independent of time).

It is difficult to find reliable data with good resolution for the latitudinal dependence of the nearshore wind. The two main sources of data were (a) the Meteorological Atlas of the Indian Ocean Expedition (Ramage, Miller, and Jeffries, 1972) and (b) Hellerman's (1967) updated estimates of the wind stress. The former suggests an almost constant wind from 10°S to north of Cape Guardafui for May, while the latter shows the longshore wind stress increasing almost linearly from 7.5°S to 7.5°N and then attaining a peak at around 10°N. This peak is consistent with the existence of the low level jet which crosses the coast at about 9°N and then blows

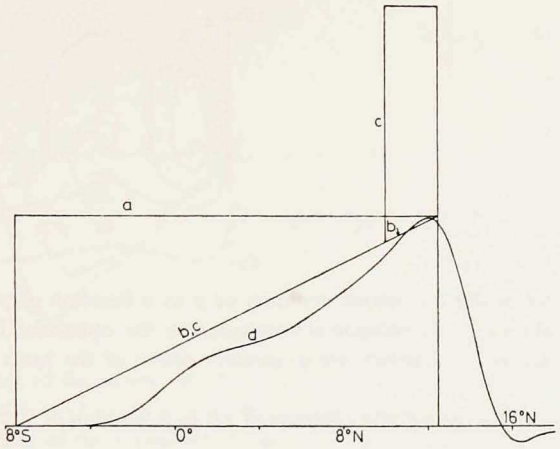

Figure 1. Plot of three (*a,b,c*) possible longshore wind stress profiles as a function of *y* and an analytic approximation to *b* as given by Eq. (5.1).

parallel to the coast over the ocean (Findlater, 1974; Duing and Szekielda, 1969; Saha, 1974). The three profiles used in the model to approximate these (the latter both with and without the low level jet) are shown in Fig. 1.

In Figs. 2a,b are shown the resulting longshore velocity and displacement of the thermocline as functions of *y* at the coast (from equations 3.4-3.6). The points of interest are (noting that negative *p* corresponds to upward thermocline displacement):

(i) North of the equator the upwelling in all cases is rather similar, although the

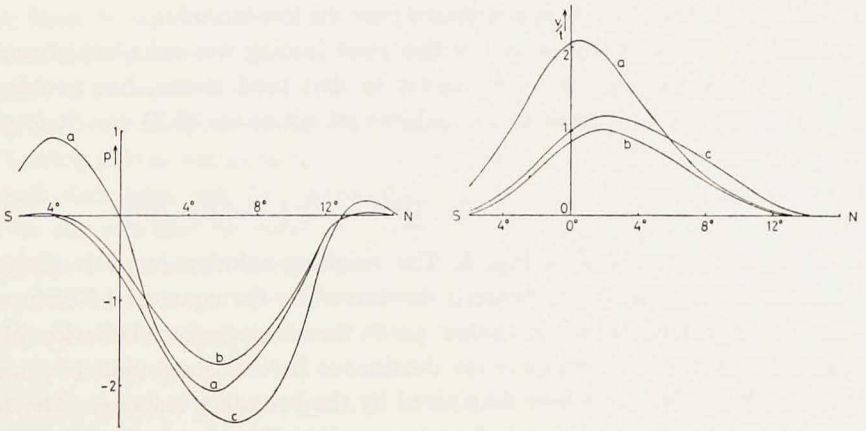

Figure 2a. (left) Plot of the asymptotic form of p at $x = 0$ as a function of y for the three longshore wind stress profiles given in Fig. 1.

Figure 2b. (right) As for 2a but for v/t.

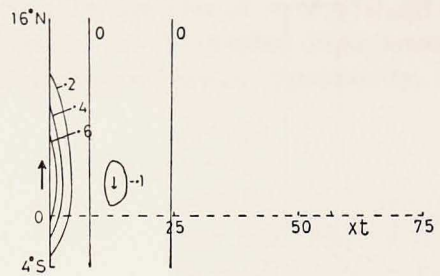

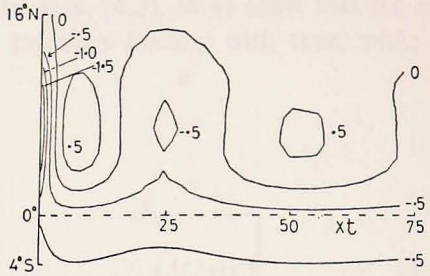

Figure 3a. (right) Plot of the asymptotic contours of p as a function of y, xt for curve d of Fig. 1. For small values of y the solution is dominated by the equatorial Kelvin wave but for larger values of y, the short planetary waves produce eddies of the form $J_0[(2xt)^{\frac{1}{2}}]$. The contour interval is .5.

Figure 3b. (left) Plot of the asymptotic contours of v/t as a function of y, xt.

stress profiles are very different. In particular, there is no local upwelling maximum where the stress is greatest.

(ii) In the southern hemisphere there is upwelling for profile 1a but downwelling for 1b.

(iii) Longshore velocity contours are similar, but the maximum flow varies with the forcing profile, both in amplitude and position ($\frac{1}{2}$°N-2°N).

Some of these points are qualitatively explicable in terms of Ekman flux arguments modified to account for Kelvin waves. In the northern hemisphere one expects a northward wind stress to drive upwelling, whose amplitude increases as $1/f$ toward the equator, and a corresponding northward geostrophic current (at least away from the equator). Coastal Kelvin waves move equatorward, which explains the lack of large response at $y = 6.25$ when the wind stress is a maximum there. Thus the effect of this peak in the forcing is distributed over the low latitudes.

The solution away from the coast for this local forcing was calculated from the theory of §3. The forcing used was similar to that used above, but avoids any difficulties due to discontinuities in the differential equations (3.8) etc. It is given by

$$Y = 2 \exp[-(6+y^2)(y-6)^2/100] - \exp[-0.42(y-6)^2] \tag{5.1}$$

and is illustrated by curve d in Fig. 1. The resulting solution for p is shown in Fig. 3a. Near the equator the response is dominated by the equatorial Kelvin wave (almost independent of xt) while farther north the characteristic behavior of the Bessel function is manifest, implying the dominance here of short planetary waves. In fact, the solution is everywhere dominated by the boundary response. The zonal velocity u may be derived from q and r. An equation for v is obtained from (2.3) as in (3.14). The result is shown in Fig. 3b. From 3a and 3b it is apparent that v and p are geostrophically balanced.

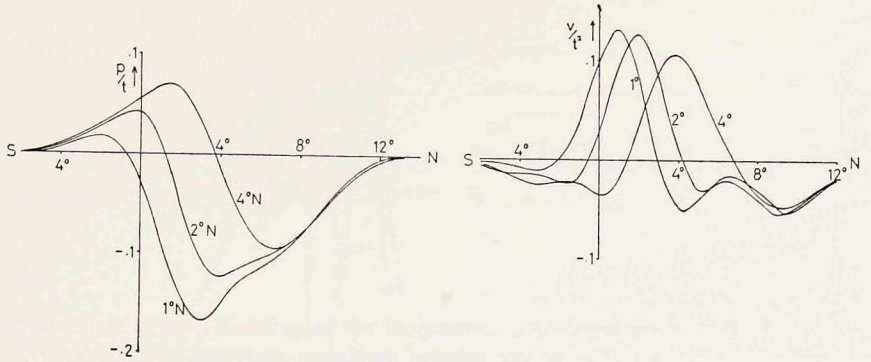

Figure 4a. (left) Plot of the asymptotic form of p/t at $x = 0$ versus y for forcing of the form (5.2) for values of $b = \cdot 5, 1, 2$ i.e. for east-west forcing north of 1°, 2°, 4°N respectively.

Figure 4b. (right) Plot of the asymptotic form of v/t^2 at $x = 0$ as a function of y for the same values of b. Note that there is little difference in the intensity of the longshore flow for varying values of b, though the position of maximum flow moves northward.

The results of §4 are now applied to the remote forcing. Again reliable data on the wind stress are difficult to find. Hellerman (1967) suggests a maximum intensity of about .5 dynes cm^{-2} at about 57½°E, but his 5° resolution does not enable us to establish the latitude of maximum forcing very accurately. Lighthill (1969) suggests that this is 2°N which seems consistent with Ramage *et al.* (1972). However, because of the uncertainty in the forcing it is necessary to examine the sensitivity of results to various types of forcing. We will consider forcing of the form

$$X = H(x-a)\, H(y-b)\, H(t) \tag{5.2}$$

where H is the Heaviside function, a is the distance from the coast and b the distance from the equator at which the forcing is applied.

Results for p at $x = 0$, calculated as in §4, are shown in Fig. 4a, for $b = \cdot 5,1,2$. A point of importance here is that the shape of the upwelling curves are very similar, with downwelling south of the equator and upwelling in the forced region. As the forcing moves northward, so does the region of maximum upwelling, and its strength decreases, but the downwelling intensifies as it moves northward. From Fig. 4b one sees that the maximum longshore flow is at 1°, 2°, 4°N, i.e. maximum velocity corresponds with the region of maximum pressure gradient in the y direction which in turn corresponds with the maximum y gradient of the forcing. The amplitude of the longshore flow does not appear to be overly sensitive to the position of the forcing region, i.e. curves b, c are rather similar to curve a displaced northward by 1°, 3° respectively. It should be noted that there are no apparent discontinuities in these solutions because they were calculated by summing explicitly the series given by (2.4), (4.1), (4.2) to a finite number of terms. In fact, it is easily shown from (4.5), (4.7) and (4.8) that $\tilde{q}_I$ and $\tilde{r}_I$ have equal and opposite discon-

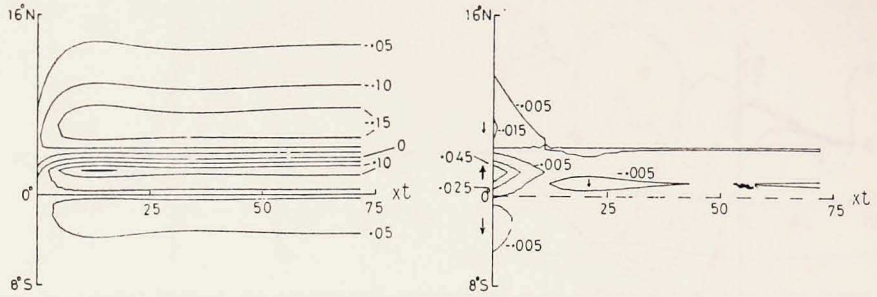

Figure 5a. (left) Plot of the asymptotic contours of p/t as a function of y, xt for forcing of the form (5.2) with $b = 1$. The interior solution dominates except near the boundary.
Figure 5b. (right) As for 5a but for v/t^2.

tinuities and thus $\bar{p}_I$ is continuous. Similarly $\bar{p}_B$ is continuous. Thus the absence of discontinuities in Fig. 4a is real and not just an effect of truncating the series. A similar argument applies to v. Of course, a large number of terms in these expansions is of dubious merit since the higher the order of the planetary wave stimulated (in a region away from the coast) the longer the time it takes to arrive at the coast. For this reason it is important to consider the proper time evolution of the solution in this case. This is done below. Meanwhile, the x-dependent asymptotic solution is shown in Fig. 5a for p and Fig. 5b for v. These were calculated using the differential equations given in §4. Away from the boundary the p-field is dominated by the interior solution set up by the long planetary waves and in this region the north-south velocity tends to be zero. There is, once again, no discontinuity in either p or v. This is necessary from the original differential equations for u, v, p given in Anderson and Rowlands (1976). In these equations, y-derivatives of p and v appear and thus any discontinuity in these leads to a delta-function appearing in the equations, which cannot be balanced by any other term. However, u is a discontinuous function of y, but this is not plotted here. An important point in Fig. 5 is that the maximum upward thermocline displacement is further north in the interior ($\sim y = 3$ i.e. 6°N) than it is at the coast ($\sim y = 2$ i.e. 4°N). The region of maximum downward thermocline displacement in the interior lies along the latitude of discontinuity in the forcing (i.e. $y = 1$).

For completeness, the effects of a westward wind stress south of the eastward wind stress is examined using forcing of the form

$$X = H(x-a)\,H(t)[H(y-b) - H(b-y)] \tag{5.3}$$

Fig. 6 shows the asymptotic forms of p/t, v/t^2 at the coast for the case $b = 1$. This figure shows that the effects are very dramatic in that the velocity maximum at ~ 2°N is almost tripled in magnitude and the downwelling very much strengthened.

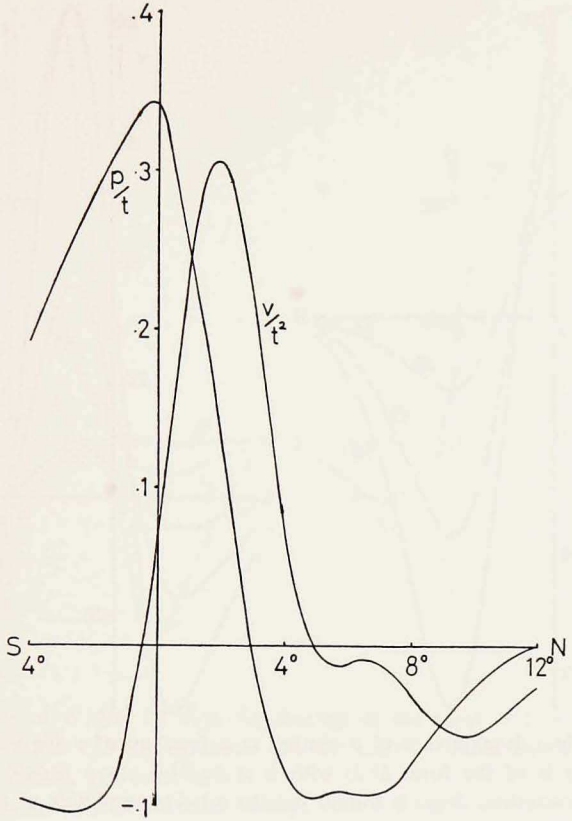

Figure 6. Plot of the asymptotic forms of p/t, v/t^2 for east-west forcing of the form (5.3) for $b = 1$.

The more detailed time development is now considered. It is expected that the above asymptotic solutions will become effective soon after the coastal Kelvin wave from the northernmost point of the local forcing has reached the equator. This takes about 6 days. Calculations show that this is indeed the case for local forcing. However, the dispersion of the equatorial waves generated by remote forcing makes further investigation of this regime necessary. For this purpose the equations were solved by numerical inversion of the Laplace transform (Lanczos 1957).

In Fig. 7a is given the solution for p and a function of time at the coast for the case when the parameters in (5.2) are $a = 3$, $b = 1$. Planetary waves will arrive at the coast after 9, 15, 21 days, etc. The general shape of Fig. 7a is similar to the asymptotic solution, but the maximum displacements of the thermocline are very different. However, the tendency for the upward displacement peak to dominate over the downward displacement with time is clearly manifest in Fig. 7a. The long-

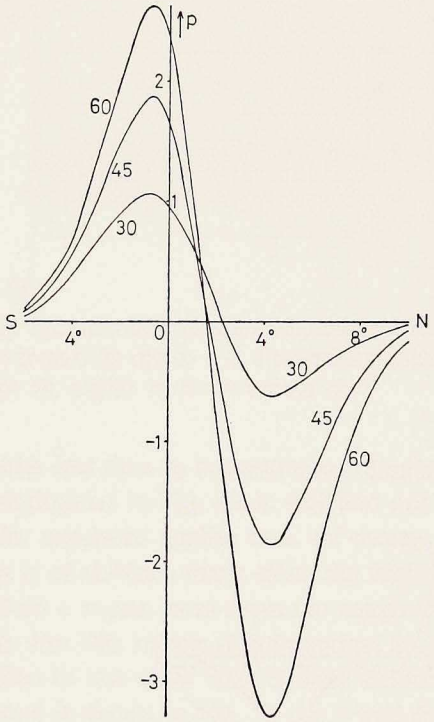

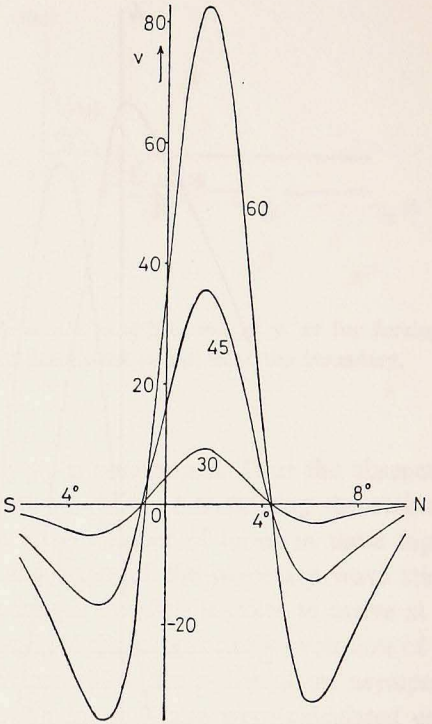

Figure 7a. (left) Time development of p plotted as a function of y for values of t = 30, 45, 60 days. Forcing is of the form (5.2) with b = 1. This curve should be compared with Fig. 4a. The characteristic shape is similar but the relative amplitude of the upwelling/downwelling differs.

Figure 7b. (right) As for Fig. 7a but for v. Comparison with Fig. 4b shows that the relative maximum amplitudes of the northerly, southerly flow differ from that given by the asymptotic solution, but the profile is qualitatively very similar. At time 45, the solution is not yet building up quadratically with time.

shore velocity plotted in Fig. 7b shows the same effect. Finally, Figs. 8a, b show the longshore flow at times 25, 75 for a = 1, 3, 5 and b = 1. After 25 days the boundary current for a = 5 is still tiny compared with a = 1; by 75 days it has grown very considerably relative to the a = 1 case but is still only approximately half as big.

6. Discussion

From the above results it is possible to make certain predictions about the Somali current response and the upwelling, downwelling to be expected. For both local and remote forcing (for the case b = 1, corresponding to an eastward wind stress north of 2°N), the longshore current is always northward between 1°S and 4.5°N (y = −.5, 2.25) but north of 4.5°N and south of 1°S, the resultant velocity

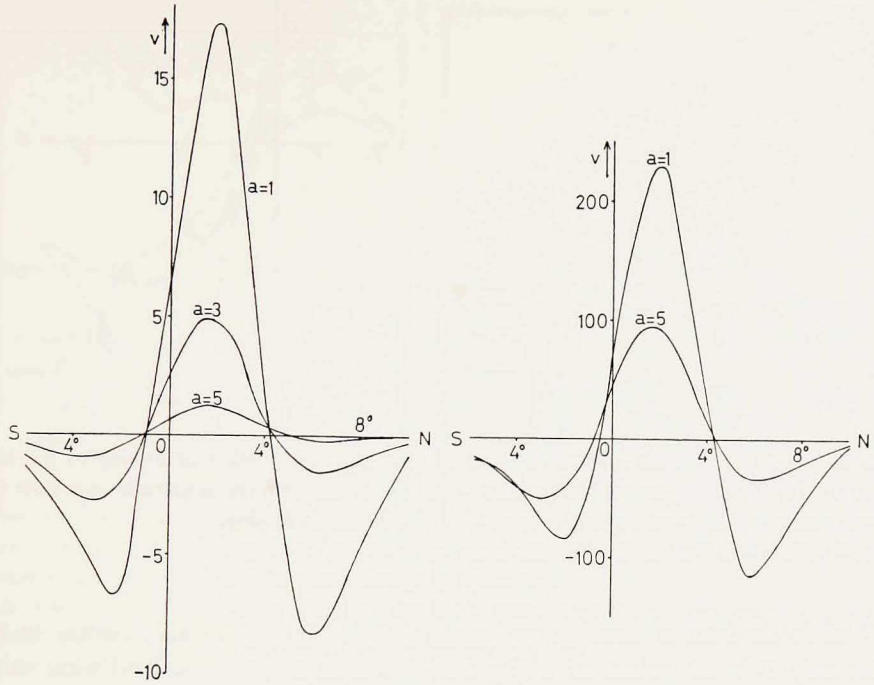

Figure 8a. (left) Plot of v after 25 days for forcing of the form (5.2) when the distance a from the coast is varied. The chosen values of a are 1,3,5 corresponding to forcing of 2°, 6°, 10° away from the coast. The value of b is 1.

Figure 8b. (right) As for Fig. 8a but after 75 days.

will be a function of time since it is a balance between opposing tendencies, the local response trying to drive a longshore flow which is northward, the response to remote forcing being southward. This implies that initially, the Somali current would be northward from say 6°S right up to Cape Guardafui (12.5°N) since the local response is dominant initially. But, if the monsoon persists long enough, the response to remote forcing will dominate (since v increases like t^2 in this case compared to t for local forcing) and then the Somali current will flow northward only from 1°S to 4.5°N. But for intermediate times it can flow northward over any value of latitude between 6°S and 12.5°N. The position at which the flow comes to zero will correspond to a separation point of the Somali current and this can move equatorward from 12.5°N to 4.5°N. Exactly how it moves cannot be determined until the relative strengths of the local and remote forcing functions are specified.

Here we strike a problem, for no very reliable data on mean wind stress is available. Hellerman's data would suggest that the longshore stress is stronger than the interior stress, appropriate values for the longshore stress at 10°N being ~ 2 dynes

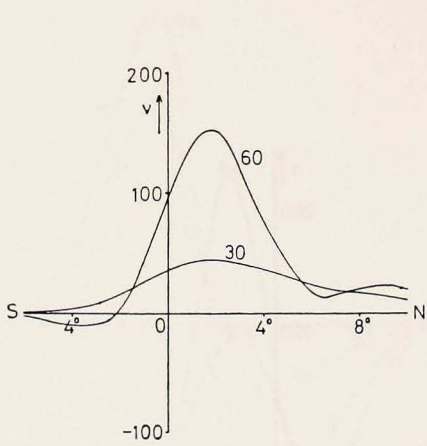

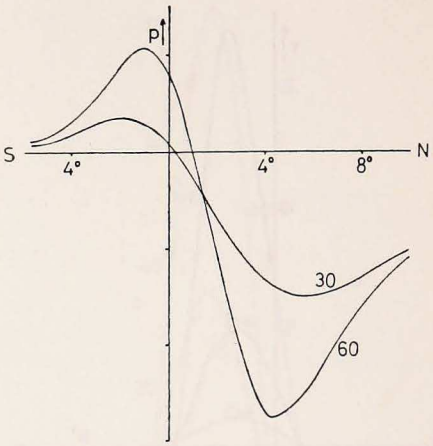

Figure 9a. (right) Resultant p curves 30 and 60 days after application of forcing of the form given by Fig. 1c and equation (5.2) with $a = 3$, $b = 1$. The relative amplitudes are such that the maximum of the local forcing is twice that of the remote forcing.

Figure 9b. (left) As for Fig. 9a, but for v.

cm^{-2} while the interior stress is $\sim$ 1 dyne cm^{-2}. But it is an easy matter to find significantly different estimates: Duing and Szekielda suggest sustained wind values in the vicinity of Cape Guardafui, presumably due to the low level jet mentioned previously, of order 17m s^{-1} which would give a wind stress of order 8 dynes cm^{-2}. Bruce (personal communication) and Stommel (personal communication) can also support moderately high stress values in this region. For the eastward wind stress in the interior, Lighthill takes a value of 2.5 dynes cm^{-2}. For the sake of comparison we take a longshore forcing of the form Fig. 1c with the maximum value twice the value of the east-west forcing in the interior. This probably underestimates the relative strength of the local forcing particularly near Cape Guardafui. The resultant p and v profiles for $X = 0$ are given in Figs. 9a,b respectively. The eastward forcing is of the form (5.2) with $a = 3$, $b = 1$, i.e., the forcing is restricted to 6°E of the coast and 2°N of the equator. The curves are plotted thirty and sixty days after the switch on of the winds which we arbitrarily took to be coincident, though Leetmaa (1972, 1973) suggests that the local winds start a few days before the interior winds.

Initially there is upwelling over the whole of the region 6°S to 12°N but after thirty days there is weak downwelling south of the equator due to the remote forcing. North of the equator the upwelling, maximized initially at 6°N, moves equatorward slightly (to 5½°N after 30 days to 4½°N after 60 days), and intensifies. For v, initially the flow is northward at all latitudes and this state of affairs persists to at least 60 days. A flow reversal, i.e., a separation point, would require about 70 days or a larger relative amplitude for the remote forcing. The position of the

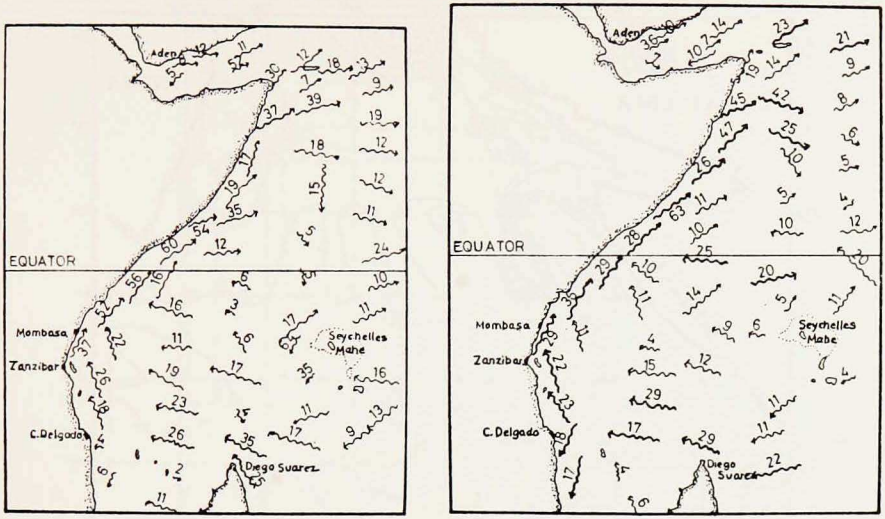

Figure 10a. (left) Average surface currents for months (a) Apr., May, June. From Indian Ocean Currents (1966). Figures give velocity in miles/day.

Figure 10b. (right) As for Fig. 10a, but for July, Aug., Sept. Note how much sharper the velocity maximum at ~ 2°N is here than in 10a. Cf. Fig. 9b.

separation point is at 6.4°N, some 2° too far to the south. It will be argued later that the separation point is not formed by this mechanism but by nonlinear response of the coastal Kelvin wave to the local wind stress. Before discussing that aspect it is interesting to see what features of the model appear to be observable in the data. Duing and Szekielda (Fig. 3, 1971) give satellite pictures of the estimated sea surface temperatures and these confirm the existence of an upwelling region at about 7°N while Figs. 6 & 7 of La Violette and Chabot (1968) (also based on satellite observations) and Fig. 4a of Bruce (1973) would suggest there was upwelling at ~ 5°N, this being more intense in August than in May. These observations appear consistent with Fig. 9a in principle.

The variability in the position of the upwelling region from year to year may possibly be accounted for by a slight change in the relative positions and intensities of the forcing functions. For example, there is evidence that the monsoon was both later and stronger in 1964 than it was in 1963, (Ramage *et al.*, 1972). Sea surface temperature charts for lower latitudes are given in this atlas. They show weak downwelling at approximately the predicted latitudes (centered at ~ 2°S) again consistent with Fig. 9a. Velocities are less easily compared on an individual month/year basis but charts of velocities averaged over several years are available for the 3-monthly periods May, June, July and August, September, October (Indian Ocean Currents, 1966). In the former the current is northward at all latitudes, being maximized at 1°N, but this is a rather flat maximum (60 miles/day) the current being

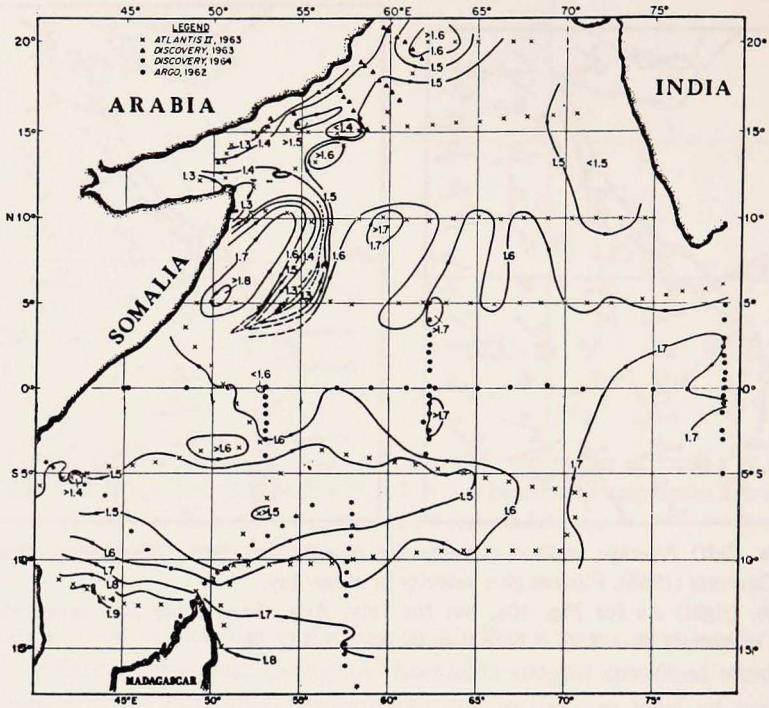

Figure 11. Contours of geopotential topography of sea surface relative to 1000 db during the Southwest Monsoon. Units are dynamic meters. From Bruce (1968). Cf. Fig. 3a.

strong from about 5°S to 4°N (where there is a hint of an eastward branching). In the latter the current maximum (63 miles/day) is very much sharper, now having moved north to 3°N. Beyond this peak the current decreases to a minimum (26.3 miles/day) at 5°N; there is an eastward branching of the current at 8°N with northerly flow beyond (maximum 19.3 miles/day). The whole picture gained from the above is encouragingly similar to Figs. 9a,b. For comparison, these charts are included as Figs. 10a,b.

The only detailed picture of upwelling away from the coast that we have found is that of Bruce (1968, Fig. 3) reproduced as Fig. 11. This appears to be very similar to that of Fig. 3a. If that is so the implication is that local forcing may have a more important effect than remote forcing in stimulating offshore "eddies". Certainly, short planetary waves traveling at 1/8 ms^{-1}, if not strongly damped, penetrate as far as 15° from the coast in 3 months. Fig. 3a implies that these eddies migrate westward. There seems to be no observational evidence about this point.

The linear model does not give good agreement with observation in the region north of Ras Hafun. Swallow & Bruce (1966), La Violette & Chabot (1968), Bruce (1968, 1970, 1973, 1974), Duing & Szekielda (1970), and Ramage *et al.*

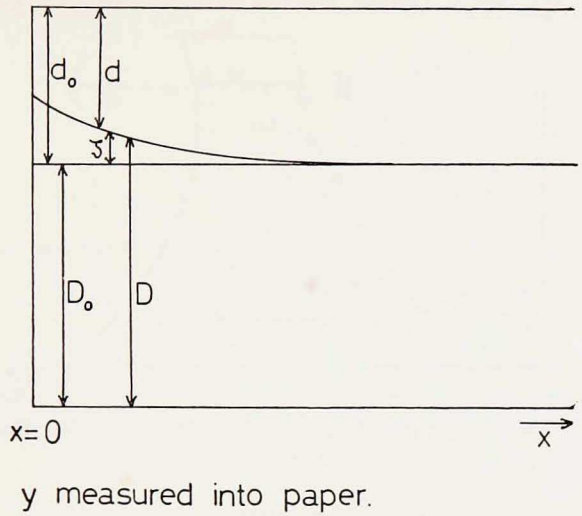

Figure 12. Specification of the two-layer model parameters.

(1972) all support the existence of strong upwelling centered at 11°N. There is nothing in this model to give such strong upwelling. Indeed, from Fig. 9a one would conclude that though there would be upwelling there, it would be weaker than farther south. Clearly this is inconsistent with the observations. However Duing & Szekielda (1971), Hellerman (1967), and Findlater (1974) all suggest that the forcing is much stronger in this region than elsewhere. But Fig. 2a shows that Kelvin waves carry the upwelling to lower latitudes leaving no residual upwelling to correlate with the local forcings. On this picture there can be no local response. Initially this picture is probably correct. But upwelling tends to generate a long-shore flow (geostrophically balanced with the upwelling pressure gradient). This mean current opposes the Kelvin wave propagation, tending to retard the Kelvin wave, forcing it to remain longer and longer in the forcing region and providing a mechanism for feedback. This problem of analyzing the behavior of a forced Kelvin wave interacting with a mean flow for general stratification is essentially nonlinear; modal decomposition cannot in general be used but the simpler problem using a two-layer model is solved in the Appendix. The analysis shows (see Fig. 13) that the mechanism suggested above is correct and that the effects of the mean flow set up by the Kelvin wave act to retard its equatorward propagation.[2] This makes it possible for a local response to develop. The equations become singular (in the sense that the upper layer depth becomes zero) when the speed of the fluid in the top layer is exactly equal and opposite to the velocity of the Kelvin wave.

2. Cox (1976) in a sophisticated nonlinear numerical model of the Somali current also observes this effect.

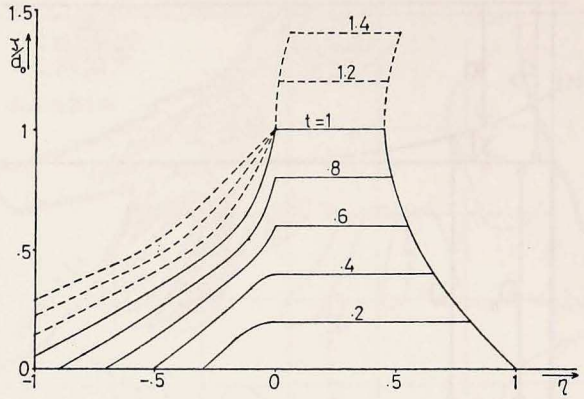

Figure 13. Plot of dimensionless upwelling for the nonlinear model. Dashed lines are for times such that the top layer has negative depth.

APPENDIX

Nonlinear coastal Kelvin waves—the upwelling region off Cape Guardafui

The analysis, which is similar to that of Bennett (1973) who studied barotropic coastal Kelvin waves, will be performed on an f-plane, as the region of interest is sufficiently far from the equator and of a sufficiently small meridional extent to make this valid. The model ocean consists of an upper layer of depth d_0 and a lower layer of depth D_0 initially. The density of the upper layer is ρ and that of the lower layer is ρ'. The vertical displacement of the interface is ξ (positive upward) and the depths of the upper and lower layers are d,D respectively. Thus we have $d = d_0 - \xi$ and $D = D_0 + \xi$. The barotropic pressure is ϕ; g is acceleration due to gravity and $g' = g(1 - \rho/\rho')$ is the reduced gravity. The ocean surface and bottom are horizontal and rigid, and the coast ($x = 0$) is plane and vertical. x is measured positive toward the interior of the ocean and y is the coordinate along the coast, (u,v), (u',v') are the (x,y) components of velocity in the upper and lower layers respectively (see Fig. 12). The forcing mechanism will be taken as a body force Y uniformly distributed throughout the upper layer and independent of x; this last approximation has been justified above. In reality, for a given wind stress on the ocean surface the body force in the upper layer will be inversely proportional to the depth of that layer, and as we will be considering upwelling which brings the interface very near the surface, this should really be taken into account in the model. However, to do so makes the problem intractable and so the effect is not considered. In fact, it is apparent that this effect will not alter the main conclusion that upwelling is much greater in the forcing region (and possibly to the north of it) than it is farther south.

With the above definitions the equations of motion for the upper layer are:

$$\begin{gathered} -fv + \phi_x = 0 \\ v_t + uv_x + uv_y + fu + \phi_y = Y(y,t) \\ (du)_x + (dv)_y - \xi_t = 0 \end{gathered} \tag{A.1}$$

and for the lower layer:

$$\begin{gathered} -fv' + g'\xi_x + \frac{\rho}{\rho'}\phi_x = 0 \\ v'_t + u'v'_x + v'v'_y + fu' + g'\xi_y + \rho/\rho'\,\phi_y = 0 \\ (Du')_x + (Dv')_y + \xi_t = 0\ . \end{gathered} \tag{A.2}$$

Equations expressing the conservation of potential vorticity in the upper and lower layers separately are

$$\left(\frac{\partial}{\partial t} + u\frac{\partial}{\partial x} + v\frac{\partial}{\partial y}\right)\left(\frac{v_x + \mathrm{f}}{d}\right) = 0 \tag{A.3}$$

and

$$\left(\frac{\partial}{\partial t} + u'\frac{\partial}{\partial x} + v'\frac{\partial}{\partial y}\right)\left(\frac{v'_x + t}{D}\right) = 0 \ . \tag{A.4}$$

Hence, as the ocean is initially at rest with d and D uniform, we obtain

$$d_0 v_x + f\xi = 0 \tag{A.5}$$

and

$$D_0 v'_x - f\xi = 0 \ . \tag{A.6}$$

Substituting for v and v' from the first of the momentum equations then gives

$$\phi_{xx} + f^2/d_0\,\xi = 0 \tag{A.7}$$

and

$$\rho/\rho'\,\phi_{xx} + g'\,\xi_{xx} - \frac{f^2}{D_0}\,\xi = 0 \ . \tag{A.8}$$

The general solution of these equations is

$$\begin{aligned} \xi &= Z(y,t)e^{\lambda x} + Z'(y,t)e^{-\lambda x} \\ \phi &= \Phi(y,t)e^{\lambda x} + \Phi'(y,t)e^{-\lambda x} + A(y,t)x + B(y,t) \end{aligned} \tag{A.9}$$

where

$$\lambda^2\Phi = -\frac{f^2 Z}{d_0}$$

and

$$\lambda^2\Phi' = \frac{-f^2}{d_0}\,Z'$$

and λ is the negative square root of $\frac{f^2}{g'}\left(\frac{1}{D_0} + \frac{\rho}{\rho' d_0}\right)$. We want solutions which are bounded as $x \longrightarrow \infty$. Thus we have

$$\xi = Ze^{\lambda x} \tag{A.10}$$

and

$$\phi = \Phi e^{\lambda x} + B$$

The boundary condition that $u = u' = 0$ at $x = 0$ gives, via the momentum equations:

$$\frac{\lambda}{f}\,\Phi_t + \frac{\lambda^2}{\rho^2}\,\Phi\,\Phi_y + \Phi_y + B_y = Y \tag{A.11}$$

and

$$\left(1 - g'd_0\,\frac{\rho'}{\rho}\,\frac{\lambda^2}{f^2}\right)\left[\frac{\lambda}{f}\,\Phi_t + \frac{\lambda^2}{f^2}\left(\frac{\rho}{\rho'} - d_0 g'\,\frac{\lambda^2}{f^2}\right)\Phi\,\Phi_y + \Phi_y\right] = -B_y \ .$$

These equations can be solved as they stand to give a (complicated) nonlinear equation for Φ. However they can be simplified by noting that in the real ocean $D_0 >> d_0$ and $1 - \rho/\rho' \cong 0$. These approximations give $\lambda \sim -f/(g'd_0)^{\frac{1}{2}}$ and the last two equations become

$$B_y = 0 \tag{A.12}$$

and

$$\Phi_t - c\Phi_y - \frac{1}{c}\,\Phi\,\Phi_y = -\,cY$$

where

$$c = (g'd_0)^{\frac{1}{2}} .$$

This may be cast into a more standard form by defining

$$\eta = y/c \tag{A.13}$$

and

$$\zeta = 1 + \Phi/c^2 .$$

Then we obtain

$$\zeta_t - \zeta\zeta_\eta = -\,Y/c \tag{A.14}$$

with $\zeta = 1$ at $t = 0$.

It should be noted that the equation for Φ is just the same as that obtained by Bennett (1973) in the barotropic case.

General solution of the equation $\zeta_t + \zeta\,\zeta_\eta = -\,f(\eta)$

As with the linear analysis given earlier we are interested in the response to a steady wind suddenly imposed at $t = 0$. Thus we wish to study the solutions of the equation

$$\zeta_t - \zeta\,\zeta_\eta = -\,f(\eta) \tag{A.15}$$

with

$$\zeta = 1 \text{ at } t = 0 .$$

Defining characteristic coordinates

$$X = \eta + \int_0^t \zeta\,dt \tag{A.16}$$

and

$$T = t ,$$

we obtain the pair of simultaneous equations

$$\left.\frac{\partial\eta}{\partial T}\right|_x = -\,\zeta \tag{A.17}$$

and

$$\left.\frac{\partial\zeta}{\partial T}\right|_x = -\,f(\eta) .$$

These equations are the most convenient for calculating numerical solutions. However, an analytical solution may also be obtained. We have

$$\left.\frac{\partial^2\eta}{\partial T^2}\right|_x = f(\eta) .$$

But it is easily shown that

$$\left.\frac{\partial^2\eta}{\partial T^2}\right|_x = -\left.\frac{\partial^2 T}{\partial\eta^2}\right|_x \left(\left.\frac{\partial T}{\partial\eta}\right|_x\right)^{-3} \tag{A.18}$$

and thus we have

$$\left.\frac{\partial^2 T}{\partial\eta^2}\right|_x = -\left(\left.\frac{\partial T}{\partial\eta}\right|_x\right)^3 f(\eta) . \tag{A.19}$$

This is a first order equation for $\left.\frac{\partial T}{\partial \eta}\right|_x$ and has the solution

$$\left(\left.\frac{\partial T}{\partial \eta}\right|_x\right)^2 = \left\{1 + 2\int_{\eta_0}^{\eta} f(p)dp\right\}^{-1} \tag{A.20}$$

where

$$\eta = \eta_0 \text{ at } T = 0 \ .$$

But

$$\left.\frac{\partial T}{\partial \eta}\right|_x = -\frac{1}{\zeta} \ . \tag{A.21}$$

Hence

$$\zeta(\eta) = \left[1 + 2\int_{\eta_0}^{\eta} f(p)dp\right]^{\frac{1}{2}}$$

and

$$t = T = \int_{\eta_0}^{\eta} ds/\eta_0|\zeta(s)| \tag{A.22}$$

for $t < t_c$, the time at which ζ first becomes zero. For our purpose there is no need to take the solution beyond $t = t_c$, for $\zeta = 0$ corresponds to $Z = d_0$, that is at $t = t_c$ the interface breaks the surface somewhere and the above analysis breaks down. Also at $t = t_c$ we have

$$v = ce^{\lambda x}$$

and so t_c is the time at which the speed of the current in the upper layer first equals the speed of propagation of coastal Kelvin waves.

Probably the most important conclusion to be drawn from this analysis is that to the south of the forcing region ζ can never become zero. For in a region where no forcing occurs ζ is constant along characteristics with slope $-\zeta$ in $\eta - t$ space. Thus if $\zeta = 0$ somewhere in such a region then it remains zero at that value of η for all time (i.e. $\zeta_t - \zeta\,\zeta_\eta = 0$ and $\zeta = 0$ imply $\zeta_t = 0$) and it must also have been zero at all previous times, which contradicts the initial conditions that $\zeta = 1$ at $t = 0$.

This argument is valid even for times greater than t_c; but it does not necessarily apply to regions to the north of any forcing. If we treat the differential equation purely as a mathematical problem and allow ζ to become negative then for times greater than t_c, v can become larger than c and information from the forcing region can be carried northward! But in the forcing region ζ can become negative and such values may propagate out of the forcing region to the north. However, in the physical problem, negative ζ is meaningless and the above analysis breaks down as soon as ζ becomes zero, as the wind stress forcing then acts on the lower layer in at least part of the forcing region. There is no way of telling whether ζ can subsequently become negative to the north of the forcing region. It must be emphasized however that the conclusion that ζ is positive everywhere south of the forcing region is true for all time even after the analysis has become invalid in the forcing region. The meaning of this result for our purposes is that upwelling to the south of a region of wind-stress forcing must be weaker than it is in the forcing region. This should be contrasted with the linear analysis where the upwelling is governed by the equation $\zeta_t - \zeta_\eta = -f(\eta)$ and where the upwelling south of the forcing region can be just as vigorous (albeit at some later time) as that in the forcing region; there is no upper limit to the upwelling south of the forcing region in this case.

A second important observation is that overturning of the interface only occurs for $\zeta < 0$ and so for t less than t_c the interface never overturns and thus breaking and mixing are not inevitable.

Of course in reality the wind stress is nonzero all along the coast and there is no region "south of the forcing region". However the low level jet which blows off Cape Guardafui is very much stronger than the other winds and thus upwelling will occur much more rapidly in this area. The generalization of the above result to this case is that the interface first breaks the surface as a result of local winds or winds to the south. Thus upwelling in the region of Cape Guardafui is likely to be much stronger much sooner than farther south.

As an example of the kind of upwelling obtained as a solution of the above equation, the displacement of the interface at $x = 0$ is plotted in Fig. 13 as a function of η and t for $t \leq t_c$ (=1) for

$$f(\eta) = 1 \qquad (0 < \eta < 1)$$

$$= 0 \qquad \text{elsewhere}$$

The solution for $t > t_c$ is also plotted (broken lines) for a few values of t to illustrate the fact that for negative η, ζ is less than d_0 for all time.

REFERENCES

Abramowitz, M., and I. A. Stegun. 1965. Handbook of mathematical functions, Dover, 1046 pp.

Anderson, D. L. T. 1974. A low-latitude ocean spectral model using Chebyshev parabolic cylinder functions. W.G.N.E. Report No. 7. (GARP)

Anderson, D. L. T., and A. E. Gill. 1975. Spin-up of a stratified ocean with applications to upwelling. Deep-Sea Res., *22*, 583–596.

Anderson, D. L. T., and P. B. Rowlands. 1976. The role of intertia-gravity and planetary waves in the response of a tropical ocean to the incidence of an equatorial Kelvin wave on a meridional boundary. J. Mar. Res., *34*, 295–312.

Bennett, J. R. 1973. A theory of large amplitude Kelvin waves. J. of Phys. Oceanography, *3*, 57–60.

Bruce, J. G. 1968. Comparison of near surface dynamic topography during the two monsoons in the western Indian Ocean. Deep-Sea Res., *15*, 665–677.

—— 1969. A further estimate of maximum transport of the Somali current. Deep-Sea Res., *16*, 227–228.

—— 1970. Notes on the Somali current system during the Southwest Monsoon. J. of Geophys. Res., *75*, 4170–4173.

—— 1973. Large scale variations of the Somali current during the Southwest Monsoon. Deep-Sea Res., *20*, 837–846.

—— 1974. Some details of upwelling off the Somali and Arabian coasts. J. of Marine Res., *32*, 419–423.

Cox, M. D. 1970. A mathematical model of the Indian Ocean. Deep-Sea Res., *17*, 47–75.

—— 1976. Equatorially trapped waves and the generation of the Somali current. Deep-Sea Res. (to be published).

Duing, W., and K.-H. Szekielda. 1971. Monsoonal response in the western Indian Ocean. J. of Geophys. Res., *76*, 4181–4187.

Fieux, M. 1975. Establissment de la monsson de Sud-Ouest en mer d'Arabie. C.R. Acad. Sc. Paris, Ser. B, *281*, 563–566.

Findlater, J. 1974. The low-level cross-equatorial air current of the western Indian Ocean during the Northern Summer. Weather, *29*, 411–416.

Gill, A. E., and A. J. Clarke. 1974. Wind-induced upwelling, coastal currents and sea-level changes. Deep-Sea Res., *21,* 325–345.

Hellerman, S. 1967. An updated estimate of the wind stress on the world ocean. Monthly Weather Rev., *95,* 607–626. (See also *96,* 62–74).

Indian Ocean Currents. 1966. Her Majesty's Stationary Office, 2nd Edition.

Lanczos, C. 1957. Applied Analysis. London, Pitman, 1–539.

La Violette, P. E., and P. L. Chabot. 1968. Nimbus II Satellite sea surface temperatures versus historical data in a selected region: a comparative study. Deep-Sea Res., *15,* 617–622.

Leetmaa, A. 1972. The response of the Somali Current to the southwest monsoon of 1970. Deep-Sea Res., *19,* 319–325.

—— 1973. The response of the Somali Current at 2°S to the southwest monsoon of 1971. Deep-Sea Res., *20,* 397–400.

Lighthill, M. J. 1969. Dynamic response of the Indian Ocean to onset of the S.W. monsoon. Phil. Trans. of the Royal Soc. of London *A265,* 45–92.

Moore, D. W. 1968. Planetary-gravity waves in an equatorial ocean. Ph.D. thesis, Harvard University, Cambridge, Mass.

Ramage, C. S., F. R. Miller, and C. Jeffries. 1972. Meteorological Atlas of the International Indian Ocean Expedition. National Science Foundation, Washington.

Saha, K. 1974. Some aspects of the Arabian Sea summer monsoon. Tellus, *26,* 464–476.

Swallow, J. C., and J. G. Bruce. 1966. Current measurements off the Somali coast during the southwest monsoon of 1964. Deep-Sea Res., *13,* 861–888.

Whittaker, E. T., and G. N. Watson. 1952. A course of Modern Analysis, 4th Ed. Cambridge University Press, pp. 608.

Received: *10 November, 1975;* revised: *28 April, 1976.*